

A Spectrally Accurate Boundary Integral Method for Interfacial Velocities in Two-Dimensional Stokes Flow

Xu Sun and Xiaofan Li*

Department of Applied Mathematics, Illinois Institute of Technology, Chicago, IL 60616, USA.

Received 19 September 2009; Accepted (in revised version) 9 March 2010

Available online 17 May 2010

Abstract. We present a new numerical method for solving two-dimensional Stokes flow with deformable interfaces such as dynamics of suspended drops or bubbles. The method is based on a boundary integral formulation for the interfacial velocity and is spectrally accurate in space. We analyze the singular behavior of the integrals (single-layer and double-layer integrals) appearing in the equations. The interfaces are formulated in the tangent angle and arc-length coordinates and, to reduce the stiffness of the evolution equation, the marker points are evenly distributed in arc-length by choosing a proper tangential velocity along the interfaces. Examples of Stokes flow with bubbles are provided to demonstrate the accuracy and effectiveness of the numerical method.

AMS subject classifications: 45F15, 65R20, 76T10

Key words: Boundary integral method, Stokes flow, two-phase flow, weakly singular integral, spectral accuracy.

1 Introduction

Stokes flows involving interfaces have been studied extensively in the past a few decades. It has many important applications in science and engineering, such as in biomechanics, geophysics, mechanical engineering, and chemical engineering. Numerical solutions can accurately address practical questions when analytical solutions cannot be found and real experiments are hard to realize or expensive to execute. Computer simulations have become a very important tool in studying interfacial dynamics in low Reynolds number flow.

There are many numerical methods that are suitable for computing interfacial dynamics in Stokes flow, which can be divided into two categories. Sharp interface modeling, where the interface separating two fluids has zero thickness, include boundary integral methods, level set methods, immersed interface methods, volume-of-fluid and front

*Corresponding author. *Email addresses:* xsun15@iit.edu (X. Sun), lix@iit.edu (X. Li)

tracking methods among others (see [5, 8, 10, 14, 16] and the references therein). Other methods represent interfaces using a thin transition layer, such as immersed boundary methods [11], phase-field or diffused interface methods [2]. Each method has its merits and disadvantages. Location and shape of interfaces are accurately represented by boundary integral methods but topological changes are difficult to handle for this kind of interface tracking methods. In this work, we focus on the boundary integral methods to solve the interfacial dynamics problem in two-dimensional Stokes flow. The three-dimensional problem is more challenging to study especially for evolving interfaces with large deformations.

Among boundary integral methods, boundary element method is probably the most popular one in practical applications [12]. In this method, an interface is represented by a union of boundary elements. It is reliable and computationally efficient. However, it usually suffers from low order of accuracy in space, depending on the order of the elements and the quadrature employed to compute the integrals. Quadratic elements like parabolic and circular arc elements are commonly used in practice, resulting at most second-order accuracy in space. Spectral element methods [3] use higher order orthogonal polynomials on each boundary element to achieve spectral accuracy with respect to numerical integration on individual elements. However, the spectral accuracy over the entire interface is hard to achieve using spectral element methods due to geometric discontinuities at the edges of the elements. Dimitrakopoulos and Wang [3] developed a suitable interfacial smoothing based on Hermitian-like interpolations to maintain the continuities of the interface at the edges of the spectral elements. Recently, Kropinski [7] presented a boundary integral method using Fourier series to represent the interface and improved the spatial accuracy. In [7], the two-dimensional Stokes equations are reformulated based on theory of complex variables. Kropinski [7] solves the Sherman-Lauricella integral equation for a complex density function defined on the interface. The interfacial velocity is then obtained by evaluating boundary integrals of the complex density. We present a boundary integral method that also uses the Fourier representations of the interfaces but solves the velocity on the interface directly from the boundary integral formulation. Siegel [17] presents a semi-analytic method to compute the interfacial dynamics in 2D Stokes flow based on conform mapping. This approach is extremely accurate but may not be valid for interface problem with arbitrary initial shape and velocity field.

Organization of this work is as follows. The governing equations are presented in Section 2. The details of the numerical methods are given in Section 3. Two examples are studied in Section 4 to demonstrate the accuracy of the numerical schemes.

2 Statement of the problem

Consider an ambient flow with velocity \mathbf{u}^∞ past a deformable particle, as shown in Fig. 1, where Ω_1 and Ω_2 denote the regions occupied by the ambient fluid (fluid 1) and the particle (fluid 2) respectively. The governing equation is the Stokes equation combined

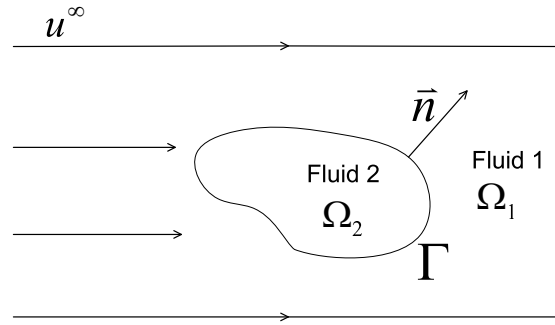


Figure 1: Sketch of an ambient flow past a deformable particle.

with the condition of incompressibility, as given below

$$\mu^i \Delta \mathbf{u}^i = \nabla P^i, \tag{2.1a}$$

$$\nabla \cdot \mathbf{u}^i = 0, \tag{2.1b}$$

where $i=1,2$, μ^1 and μ^2 are the viscosity coefficients for the ambient and particle fluids respectively. \mathbf{u}^i and P^i ($i=1,2$) are the corresponding velocities and the modified pressure, respectively. The boundary conditions on the interface Γ between the two fluids are expressed as

$$\mathbf{u}^1(\mathbf{x}) = \mathbf{u}^2(\mathbf{x}), \tag{2.2a}$$

$$[\sigma \cdot \mathbf{n}](\mathbf{x}) = \gamma \kappa \mathbf{n}(\mathbf{x}), \tag{2.2b}$$

for any $\mathbf{x} \in \Gamma$, where σ , γ , κ and \mathbf{n} are the stress tensor, surface tension coefficient, the curvature, and the unit outward normal vector, respectively. $[\cdot]$ denotes the jump across the interface.

In this work, we solve the steady Stokes equations Eq. (2.1). The variables such as the velocity \mathbf{u} depend on time t implicitly through the time-dependent interface position $\Gamma = \Gamma(\alpha, t)$, where α is the curve parameter for the interface. For cleaner presentation, we have chosen not to include time dependence in the equations, such as writing $\mathbf{u}(\mathbf{x})$ instead of $\mathbf{u}(\mathbf{x}(\alpha, t))$.

From the reciprocal identity, it can be shown that the velocity \mathbf{u} at a point \mathbf{x}_0 on the interface Γ satisfies the following Fredholm integral equation of the second kind [12]

$$u_j(\mathbf{x}_0) = \frac{2}{1+\lambda} \left(u_j^\infty(\mathbf{x}_0) - \frac{1}{4\pi\mu_1} \int_\Gamma \Delta f_i(\mathbf{x}) G_{ij}(\mathbf{x}, \mathbf{x}_0) ds(\mathbf{x}) + \frac{1-\lambda}{4\pi} \int_\Gamma u_i(\mathbf{x}) T_{ijk}(\mathbf{x}, \mathbf{x}_0) n_k(\mathbf{x}) ds(\mathbf{x}) \right), \quad j=1,2, \tag{2.3}$$

where u_j represents the velocity component in the direction of x_j -axis, and

$$G_{ij}(\mathbf{x}, \mathbf{x}_0) = -\delta_{ij} \ln r + \frac{\hat{x}_i \hat{x}_j}{r^2}, \quad T_{ijk}(\mathbf{x}, \mathbf{x}_0) = -4 \frac{\hat{x}_i \hat{x}_j \hat{x}_k}{r^4}, \tag{2.4}$$

are the Stokeslets in 2D, in which

$$\hat{\mathbf{x}} = \mathbf{x} - \mathbf{x}_0, \quad r = |\hat{\mathbf{x}}|.$$

The Einstein summation notation is used throughout this paper. $\Delta \mathbf{f} = \gamma \kappa \mathbf{n}$ is the difference of the traction across the interface, and $\lambda = \mu_2 / \mu_1$ is the viscosity ratio. It is easily seen from (2.4) that $G_{ij}(\mathbf{x}, \mathbf{x}_0)$ and $T_{ijk}(\mathbf{x}, \mathbf{x}_0)$ blow up when \mathbf{x} and \mathbf{x}_0 coincide. The numerical integration schemes for the integrals involving these singularities will be discussed in the next section.

Once the velocity \mathbf{u} on the interface is obtained, the interfacial dynamics can be determined by

$$\frac{\partial \Gamma(\alpha, t)}{\partial t} = V(\alpha, t) \mathbf{n} + T(\alpha, t) \mathbf{s}, \quad (2.5)$$

where the interface curve Γ is expressed as a 2π -periodic vector function of the parameter α and the time t , $V(\alpha, t) = \mathbf{u} \cdot \mathbf{n}$ represents the normal velocity, and \mathbf{s} is the unit tangent vector. Note that the dynamics of the interface is independent of the tangential velocity $V(\alpha, t)$ in our case. Therefore, the tangential velocity can be chosen arbitrarily. Later in this paper, it will be chosen to satisfy the equal-arclength requirement.

3 Numerical method

There are two steps in the boundary integral method for interfacial dynamics problem. The first step is to compute the interfacial velocity at each mark point on the interfaces. Then we can advance the interfaces by tracking the positions of these mark points using the evolution equation. As described below, the proposed algorithm solves the velocities on the interface at each time instant with spectral accuracy. Assuming the chosen time stepping method to solve (2.5) is k -th order accurate, then the overall error of the method can be expressed as

$$Err_{\text{overall}} = \mathcal{O}(e^{-C\Delta\alpha}) + \mathcal{O}((\Delta t)^k), \quad (3.1)$$

where $C > 0$, $\Delta\alpha$ is the spatial resolution, and Δt is the time-step size. It suggests that, for a given time t , if the time-step size Δt is sufficiently small, then the algorithm could achieve spectral accuracy with respect to space.

3.1 Boundary integral method

In this section, we shall analyze the integrals in detail by decomposing the integrals into different terms based on their smoothness, and then present a numerical method of spectral accuracy to solve the boundary integral equation (BIE) (2.3).

We first identify the interface Γ with the parameterized curve $\mathbf{x}(\alpha)$ ($0 \leq \alpha \leq 2\pi$) with counterclockwise orientation. In the following, we suppress the time dependency by writing, for example, $\mathbf{x}(\alpha, t)$ as $\mathbf{x}(\alpha)$ and denote

$$\begin{aligned} u_j(\alpha) &= u_j(\mathbf{x}(\alpha)), & u_j(\alpha_0) &= u_j(\mathbf{x}(\alpha_0)), \\ G_{ij}(\alpha, \alpha_0) &= G_{ij}(\mathbf{x}(\alpha), \mathbf{x}(\alpha_0)), & T_{ijk}(\alpha, \alpha_0) &= T_{ijk}(\mathbf{x}(\alpha), \mathbf{x}(\alpha_0)), \end{aligned}$$

and so on. Rewriting Eq. (2.3) as

$$\begin{aligned} u_j(\alpha_0) &= \frac{2}{1+\lambda} u_j^\infty(\alpha_0) - \frac{1}{(2\pi\mu_1)(1+\lambda)} \int_0^{2\pi} \Delta f_i(\alpha) G_{ij}(\alpha, \alpha_0) s_\alpha(\alpha) d\alpha \\ &\quad + \frac{\beta}{2\pi} \int_0^{2\pi} u_i(\alpha) T_{ijk}(\alpha, \alpha_0) n_k(\alpha) s_\alpha(\alpha) d\alpha, \end{aligned} \tag{3.2}$$

where

$$\beta = \frac{(1-\lambda)}{(1+\lambda)}, \quad s_\alpha(\alpha) = \left| \frac{d\mathbf{x}(\alpha)}{d\alpha} \right| = \sqrt{x_1'^2(\alpha) + x_2'^2(\alpha)}.$$

Substituting the expressions of the Green's functions (2.4) into the BIE (3.2), and rewriting

$$\ln R(\alpha, \alpha_0) = \ln \left(R(\alpha, \alpha_0) / 2 \sin \frac{|\alpha - \alpha_0|}{2} \right) + \frac{1}{2} \ln \left(4 \sin^2 \frac{|\alpha - \alpha_0|}{2} \right), \tag{3.3}$$

Eq. (3.2) becomes

$$\begin{aligned} u_j(\alpha_0) &= C_0 + C_1 \int_0^{2\pi} D_j(\alpha, \alpha_0) d\alpha + C_2 \int_0^{2\pi} E_j(\alpha, \alpha_0) d\alpha \\ &\quad + C_3 \int_0^{2\pi} F_j(\alpha, \alpha_0) d\alpha + C_4 \int_0^{2\pi} u_i(\alpha) H_{ij}(\alpha, \alpha_0) d\alpha, \end{aligned} \tag{3.4}$$

where

$$D_j(\alpha, \alpha_0) = \Delta f_j(\alpha) s_\alpha(\alpha) \ln \left[\sqrt{(x_1(\alpha) - x_1(\alpha_0))^2 + (x_2(\alpha) - x_2(\alpha_0))^2} / 2 \sin \frac{|\alpha - \alpha_0|}{2} \right], \tag{3.5}$$

$$E_j(\alpha, \alpha_0) = \Delta f_j(\alpha) s_\alpha(\alpha) \ln \left(4 \sin^2 \frac{|\alpha - \alpha_0|}{2} \right), \tag{3.6}$$

$$F_j(\alpha, \alpha_0) = \Delta f_i(\alpha) s_\alpha(\alpha) \frac{(x_i(\alpha) - x_i(\alpha_0))(x_j(\alpha) - x_j(\alpha_0))}{(x_1(\alpha) - x_1(\alpha_0))^2 + (x_2(\alpha) - x_2(\alpha_0))^2}, \tag{3.7}$$

$$H_{ij}(\alpha, \alpha_0) = \frac{(x_i(\alpha) - x_i(\alpha_0))(x_j(\alpha) - x_j(\alpha_0))(x_k(\alpha) - x_k(\alpha_0))}{\left[(x_1(\alpha) - x_1(\alpha_0))^2 + (x_2(\alpha) - x_2(\alpha_0))^2 \right]^2} n_k(\alpha) s_\alpha(\alpha). \tag{3.8}$$

The coefficients are given by

$$\begin{aligned} C_0 &= \frac{2u_j^\infty(\alpha_0)}{(1+\lambda)}, & C_1 &= \frac{1}{(2\pi\mu_1)(1+\lambda)}, \\ C_2 &= C_1/2, & C_3 &= C_1, & C_4 &= -2\beta/\pi. \end{aligned}$$

In the following, we show that if the interface curve is of $C^\infty[0,2\pi]$, then the four integrals in the right hand side of Eq. (3.4) can all be computed with spectral accuracy. First, we find the limits of the integrands when the source point \mathbf{x}_0 and the observation point \mathbf{x} coincide, i.e., $\alpha \rightarrow \alpha_0$,

$$D_j(\alpha_0, \alpha_0) = \lim_{\alpha \rightarrow \alpha_0} D_j(\alpha, \alpha_0) = \Delta f_j(\alpha_0) s_\alpha(\alpha_0) \ln(s_\alpha(\alpha_0)), \tag{3.9}$$

$$F_j(\alpha_0, \alpha_0) = \lim_{\alpha \rightarrow \alpha_0} F_j(\alpha, \alpha_0) = \Delta f_i(\alpha_0) \frac{x'_i(\alpha_0)x'_j(\alpha_0)}{s_\alpha(\alpha_0)}, \tag{3.10}$$

$$H_{ij}(\alpha_0, \alpha_0) = \lim_{\alpha \rightarrow \alpha_0} H_{ij}(\alpha, \alpha_0) = \frac{\kappa(\alpha_0)}{2} \frac{x'_i(\alpha_0)x'_j(\alpha_0)}{s_\alpha(\alpha_0)}, \tag{3.11}$$

where

$$\kappa(\alpha_0) = \frac{x'_1(\alpha_0)x''_2(\alpha_0) - x'_2(\alpha_0)x''_1(\alpha_0)}{(x'^2_1(\alpha_0) + x'^2_2(\alpha_0))^{\frac{3}{2}}},$$

is the curvature of the curve at α_0 . Then, as shown in the Appendix, if the curve Γ is of $C^\infty[0,2\pi]$, then the integrands in Eqs. (3.5), (3.7) and (3.8), are also of $C^\infty[0,2\pi]$ and periodic for any α_0 . As a consequence, the first, the third and the fourth integrals on the right-hand-side of Eq. (3.4) can be computed with spectral accuracy by using the composite trapezoidal rule for periodic integral [6]. Expressing $E_j(\alpha, \alpha_0)$ as

$$E_j(\alpha, \alpha_0) = Q_j(\alpha) \ln\left(4\sin^2\frac{|\alpha - \alpha_0|}{2}\right),$$

where

$$Q_j(\alpha) = \Delta f_j(\alpha) \sqrt{x'^2_1(\alpha) + x'^2_2(\alpha)},$$

the second integral in Eq. (3.4) can be rewritten as

$$\int_0^{2\pi} E_j(\alpha, \alpha_0) d\alpha = \int_0^{2\pi} Q_j(\alpha) \ln\left(4\sin^2\frac{|\alpha - \alpha_0|}{2}\right) d\alpha. \tag{3.12}$$

Let us divide the interval $[0,2\pi]$ of the curve parameter α evenly by $2N$ segments and denote $\omega_q = q\pi/N$, where $q=0,1,\dots,2N-1$. Choosing α_0 to be one of ω_q 's, $\alpha_0 = \omega_n$, we can approximate the weakly singular integral (3.12) with the following spectrally accurate quadrature [6]

$$\int_0^{2\pi} E_j(\alpha, \omega_n) d\alpha \approx \frac{\pi}{N} \sum_{m=0}^{2N-1} R_{|m-n|}^{(N)} Q_j(\omega_m), \tag{3.13}$$

where the quadrature weights $R_k^{(N)}$ are given by

$$R_k^{(N)} = -2 \left(\sum_{p=1}^{N-1} \frac{1}{p} \cos \frac{pk\pi}{N} + \frac{(-1)^k}{2N} \right), \quad k=0,1,\dots,2N-1. \tag{3.14}$$

Requiring the integral equation (3.2) be true at each of the quadrature points $\{\omega_n\}$ after applying the numerical integration schemes, we obtain the following system of linear algebraic equations for the velocity U_{jn}

$$U_{jn} = C_0 + \frac{\pi}{N} \sum_{m=0}^{2N-1} \left[C_1 D_j(\omega_m, \omega_n) + C_2 R_{|m-n|}^{(N)} Q_j(\omega_m) + C_3 F_j(\omega_m, \omega_n) + C_4 U_{im} H_{ij}(\omega_m, \omega_n) \right], \quad j=1,2, \quad n=0,1,\dots,2N-1, \quad (3.15)$$

where U_{jn} denotes the numerical approximation to $u_j(\omega_n)$.

Eq. (3.15) is dense and non-symmetric. The size of the linear system is twice of the number of marker points on the interface, which is usually large in applications. Consequently, the Krylov subspace iterative method GMRES is employed to solve the linear system [15].

3.2 Time-stepping method

Once the normal velocity $V = \mathbf{u} \cdot \mathbf{n}$ on the interface is obtained, the interface can be updated using Eq. (2.5). The stability constraint for integrating Eq. (2.5) with an explicit time-stepping method is

$$\Delta t = \mathcal{O}((\min s_\alpha)h),$$

where Δt is the time stepsize and h is the grid spacing in α [4, 7]. Thus, the stability constraint is determined by the minimum spacing between neighboring marker points i.e.,

$$hs_\alpha \approx \Delta s.$$

To avoid the stiffness due to the clustering of the mark points, we employ θ - L formulation to maintain the marker points at equal intervals in arclength. Following [4], the motion of the interface can be reposed in terms of the arc length derivative s_α and the tangent angle θ defined implicitly by the unit tangent vector,

$$\mathbf{s}(\alpha, t) = \frac{(x_\alpha, y_\alpha)}{s_\alpha} = (\cos\theta(\alpha, t), \sin\theta(\alpha, t)).$$

Then s_α and θ satisfy

$$s_{\alpha t} = T_\alpha + \theta_\alpha V, \quad \theta_t = \frac{T\theta_\alpha - V_\alpha}{s_\alpha}. \quad (3.16)$$

Note that the choice of the tangential velocity T does not change the shape of the interface Γ but modifies the definition of α . During the evolution of the interface curve, it is highly desirable to keep s_α constant in α , i.e.,

$$s_\alpha = \frac{L(t)}{2\pi}.$$

The following choice of T will keep α be the equal-arclength parametrization,

$$T(\alpha, t) = T(0, t) - \int_0^\alpha \theta_{\alpha'} V d\alpha' + \frac{\alpha}{2\pi} \int_0^{2\pi} \theta_{\alpha'} V d\alpha'. \quad (3.17)$$

Unlike the interface problems in Hele-Shaw flow and inertial vortex sheets, dynamics of the interface in Stokes flow is not intrinsically stiff, as noted in [7]. We find the fourth-order Adams-Bashforth multistep method works well in time integration computation for Eq. (3.16).

4 Numerical results

In this section, two examples of simulating the motion of bubbles in Stokes flow are presented. The objective of the first example is to numerically verify the accuracy of the solution to Eq. (3.15), the discretized form of the BIE (2.3). In the second example, we apply the numerical methods described in the previous section to a bubble evolution problem involving high interfacial curvature.

For bubbles, the viscosity ratio $\lambda=0$ and it is well known that the BIE (2.3) has infinite number of solutions due to the freedom of choice of the bubble volume. By specifying the bubble be incompressible, i.e.,

$$\int_{\Gamma} u_j(\mathbf{x}) n_j(\mathbf{x}) ds(\mathbf{x}) = 0, \quad (4.1)$$

Eq. (2.3) has a unique solution for $\lambda=0$. It can be shown that Eqs. (2.3) and (4.1) can be combined into one equation [9]

$$\begin{aligned} u_j(\mathbf{x}_0) = & 2u_j^\infty(\mathbf{x}_0) - \frac{1}{2\pi\mu_1} \int_{\Gamma} \Delta f_i(\mathbf{x}) G_{ij}(\mathbf{x}, \mathbf{x}_0) ds(\mathbf{x}) + \frac{1}{2\pi} \int_{\Gamma} u_i(\mathbf{x}) T_{ijk}(\mathbf{x}, \mathbf{x}_0) n_k(\mathbf{x}) ds(\mathbf{x}) \\ & + Cn_j(\mathbf{x}_0) \int_{\Gamma} u_i(\mathbf{x}) n_i(\mathbf{x}) ds(\mathbf{x}), \end{aligned} \quad (4.2)$$

where C can be any nonzero constant. Here, $C=1/L$ is chosen, where $L = \int_{\Gamma} ds(\mathbf{x})$ is the total arclength of the interface curve. Similar to the procedure of obtaining (3.15), we can get the discretized equations corresponding to (4.2) using the trapezoidal rule on the last integral term in the equation.

4.1 Verification of the order of accuracy

To verify the accuracy of the numerical methods presented in the previous section, we compute the velocity, i.e., the solution to Eq. (4.2), for an incompressible bubble immersed in a quiescent flow corresponding to $\mathbf{u}^\infty = 0$. Let the bubble have the shape of ellipse with the aspect ratio 3:1 and compare the numerical solution to the analytical solution \mathbf{u} provided in [18].

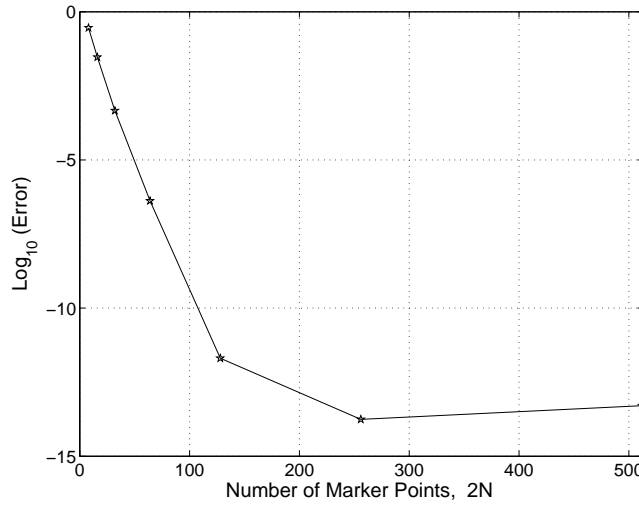


Figure 2: The maximum error in the numerical solution of the velocity, in logarithmic scale, plotted as a function of the total number of marker points $2N$. The numerical solution U_{jn} is obtained by solving Eq. (3.15) for an elliptic bubble of aspect ratio of 3 immersed in a quiescent flow, while the exact solution \mathbf{u} is provided in [18].

We define the error by

$$Error(N) = \|(\mathbf{U}(N) - \mathbf{u})\|_{\infty},$$

the maximum difference between the numerical solution $\mathbf{U}(N) = \{U_{jn}\}$ at $2N$ marker points and the analytic solution $\mathbf{u} = \{u_j(\omega_n)\}$. Fig. 2 and Table 1 show the error from the numerical solutions for the number of marker points $2N$ ranging from 16 to 512 by doubling the number of points $2N$ successively. Table 1 also shows the numerical order of convergence $Order(N)$, defined by

$$Order(N) = \log_2 \left(\frac{Error(N/2)}{Error(N)} \right).$$

Shown from the data, as the resolution increases, the magnitude of the error decreases quickly until it approaches the level of round-off error in our calculation $\mathcal{O}(10^{-14})$. Fig. 2 shows the log-plot of the error as the function of $2N$ and the decay is almost a straight line until the error is about to reach round-off, which indicates the spectral accuracy of the numerical solution in the velocity.

Table 1: The error in the numerical solution of the velocity, $Error$, and the numerical convergence order, $Order$, for different values of the total number of marker points $2N$. The numerical solution for an elliptic bubble of aspect ratio of 3 immersed in a quiescent flow, is compared with the exact solution provided in [18].

N	8	16	32	64	128	256
$Error$	2.9E-1	2.9E-2	4.6E-4	4.2E-7	2.0E-12	1.8E-14
$Order$	/	3.3	6.0	10.1	17.6	6.9

4.2 Dynamics of a bubble in an extensional flow

Accurate and efficient simulation of interfacial dynamics in Stokes flow requires not only a high-order boundary integral method but also an efficient time-stepping method. Next, we demonstrate the accuracy and efficiency of our numerical methods by studying the time evolution of a two-dimensional bubble in the extensional flow described by the following equations

$$u_1^\infty = \frac{G}{a^2} x_1 \left[a^2 + 2c_1(x_1^2 - 3x_2^2) + c_2(x_1^2 + 3x_2^2) \right],$$

$$u_2^\infty = \frac{G}{a^2} x_2 \left[a^2 + 2c_1(3x_1^2 - x_2^2) + c_2(3x_1^2 + x_2^2) \right],$$

where G is the shear rate of the incident flow, a is the equivalent radius of the bubble, and c_1 and c_2 are constants which can be chosen arbitrarily. The deformation of the bubble in the above flow field has been studied numerically in [13] and [17]. With $c_1 = 0$ and $c_2 = 0.01$, Antanovskii [1] presented the analytical solution for the steady shape of the bubble.

We simulate the evolution of a circular bubble in the extensional flow until the flow reaches steady state. In our simulation, the initial circular bubble has radius one; the capillary number Ca , as defined by $Ca = 2\mu Ga/\gamma$, is chosen to be 0.4. For this value of Ca , we find that the results are accurate when the bubble is represented by 512 marker points. The non-dimensional time step-size in the simulation is 0.0002 (the dimensionless time is defined as $t = t'G$, where t' the dimensional time), and the fourth-order Adams-Bashforth multistep method is used to solve the ODE system. Whether the flow has reached a steady state is determined by the maximum value of the normal velocity along

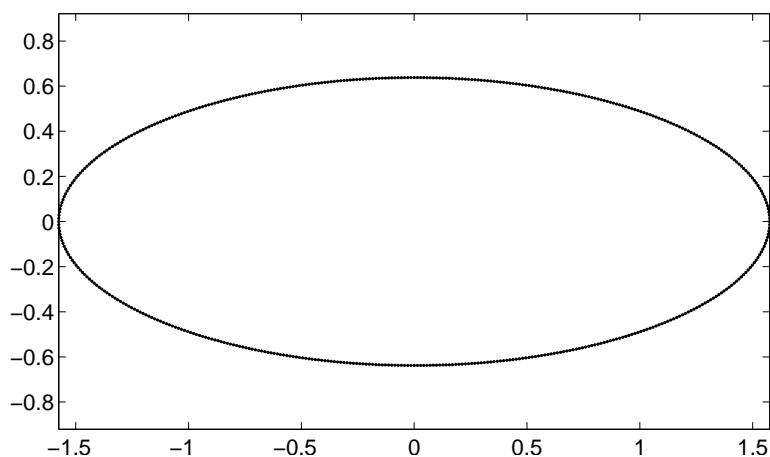


Figure 3: Comparison of the steady shapes of a bubble in an extensional flow from our numerical simulation and the analytic result in [1]. The computational shape is shown in dotted line while the exact shape is displayed in solid line.

the interface. According to our computational results, at the dimensionless time $t = 4.54$, the bubble is close to its steady shape as the non-dimensional maximum normal velocity (scaled by Ga) is less than 10^{-7} . At this moment, the curvature at the tips of the bubble is 4.041363 in our simulation (cf. the analytical value is 4.04136929459589), which has six-digit accuracy. Fig. 3 compares the final shape obtained from our computation with the analytical steady shape of the bubble given in [1], which shows the two shapes agree very well.

Acknowledgments

This work is supported by the grants NSF-DMS 0511411, 0914923 and 0923111.

Appendix: Smoothness of the integrands

We show the integrands D_j, F_j and H_{ij} in the BIE (3.4) are smooth despite they appear to be singular as their denominators vanish when $\alpha = \alpha_0$.

A.1 Case 1: when Γ is C^∞

First, it is shown that if the interface curve Γ is of $C^\infty[0, 2\pi]$, then the integrands D_j, F_j and H_{ij} defined in Eqs. (3.5), (3.7) and (3.8) are functions of $C^\infty[0, 2\pi]$. Define

$$DD(\alpha) = \sqrt{(x_1(\alpha) - x_1(\alpha_0))^2 + (x_2(\alpha) - x_2(\alpha_0))^2} / 2 \sin \frac{|\alpha - \alpha_0|}{2}, \tag{A.3}$$

$$F_{ij}(\alpha) = \frac{(x_i(\alpha) - x_i(\alpha_0))(x_j(\alpha) - x_j(\alpha_0))}{(x_1(\alpha) - x_1(\alpha_0))^2 + (x_2(\alpha) - x_2(\alpha_0))^2}, \tag{A.4}$$

$$\begin{aligned} HH(\alpha) &= \frac{(x_k(\alpha) - x_k(\alpha_0))n_k(\alpha)}{(x_1(\alpha) - x_1(\alpha_0))^2 + (x_2(\alpha) - x_2(\alpha_0))^2} \sqrt{x_1'^2(\alpha) + x_2'^2(\alpha)} \\ &= \frac{(x_1(\alpha) - x_1(\alpha_0))x_2'(\alpha) - (x_2(\alpha) - x_2(\alpha_0))x_1'(\alpha)}{(x_1(\alpha) - x_1(\alpha_0))^2 + (x_2(\alpha) - x_2(\alpha_0))^2}. \end{aligned} \tag{A.5}$$

With these definitions, the integrands can be expressed as

$$\begin{aligned} D_j(\alpha, \alpha_0) &= \Delta f_j(\alpha) \sqrt{x_1'^2(\alpha) + x_2'^2(\alpha)} \ln DD(\alpha), \\ F_j(\alpha, \alpha_0) &= \Delta f_i(\alpha) \sqrt{x_1'^2(\alpha) + x_2'^2(\alpha)} F_{ij}(\alpha), \\ H_{ij}(\alpha, \alpha_0) &= F_{ij}(\alpha) HH(\alpha). \end{aligned}$$

It is sufficient to show that $DD(\alpha)$, $F_{ij}(\alpha)$, and $HH(\alpha)$ are of $C^\infty[0, 2\pi]$. Due to assumption that the curve Γ is C^∞ , it is obvious that $DD(\alpha)$, $F_{ij}(\alpha)$, and $HH(\alpha)$ are of $C^\infty[0, \alpha_0) \cup$

$(\alpha_0, 2\pi]$. We only need to study their behavior within a sufficient small neighborhood centered around the point $\alpha = \alpha_0$.

Using the Taylor series of $x_i(\alpha) - x_i(\alpha_0)$ and $\sin|(\alpha - \alpha_0)/2|$, Eq. (A.3) become

$$\begin{aligned}
 DD(\alpha) &= \frac{\sqrt{\left[\sum_{n=1}^{\infty} \frac{x_1^{(n)}(\alpha_0)(\alpha - \alpha_0)^n}{n!}\right]^2 + \left[\sum_{n=1}^{\infty} \frac{x_2^{(n)}(\alpha_0)(\alpha - \alpha_0)^n}{n!}\right]^2}}{2 \sum_{n=1}^{\infty} \frac{(-1)^{n+1}}{(2n-1)!} \left(\frac{|\alpha - \alpha_0|}{2}\right)^{2n-1}} \\
 &= \frac{\sqrt{\left[\sum_{n=1}^{\infty} \frac{x_1^{(n)}(\alpha_0)(\alpha - \alpha_0)^{n-1}}{n!}\right]^2 + \left[\sum_{n=1}^{\infty} \frac{x_2^{(n)}(\alpha_0)(\alpha - \alpha_0)^{n-1}}{n!}\right]^2}}{1 + \sum_{n=2}^{\infty} \frac{(-1)^{n+1}}{(2n-1)!} \left(\frac{|\alpha - \alpha_0|}{2}\right)^{2n-2}}. \tag{A.6}
 \end{aligned}$$

Realizing that the denominator of the last equation does not vanish when $\alpha = \alpha_0$, i.e., $DD(\alpha)$ is actually non-singular at the point, we can obtain

$$DD(\alpha) = \sqrt{x_1'^2(\alpha_0) + x_2'^2(\alpha_0) + W(\alpha - \alpha_0)}, \tag{A.7}$$

where $W(\alpha - \alpha_0)$ is the sum of some infinite series with respect to $\alpha - \alpha_0$, which is convergent for any $\alpha \in (\alpha_0 - \delta, \alpha_0 + \delta)$ with δ being sufficiently small.

Similarly, it can be shown that

$$F_{ij}(\alpha) = \frac{x_i'(\alpha_0)x_j'(\alpha_0)}{x_1'^2(\alpha_0) + x_2'^2(\alpha_0)} + M(\alpha - \alpha_0), \tag{A.8}$$

$$HH(\alpha) = \frac{x_2'(\alpha_0)x_1''(\alpha_0) - x_1'(\alpha_0)x_2''(\alpha_0)}{x_1'^2(\alpha_0) + x_2'^2(\alpha_0)} + N(\alpha - \alpha_0), \tag{A.9}$$

where, like $W(\alpha - \alpha_0)$, $M(\alpha - \alpha_0)$ and $N(\alpha - \alpha_0)$ are of $C^\infty(-\delta, \delta)$ for sufficiently small δ . It follows from Eqs. (A.6) to (A.9) that $DD(\alpha)$, $F_{ij}(\alpha)$, and $HH(\alpha)$ are all of $C^\infty(\alpha_0 - \delta, \alpha_0 + \delta)$. Thus, in turn, the integrands in Eq. (3.4), D_j, F_j and H_{ij} are C^∞ functions for all values of α and α_0 in their domain $[0, 2\pi]$.

A.2 Case 2: when Γ is $C^k[0, 2\pi]$ ($k \geq 2$)

In this subsection, we show that if the interface curve Γ is of $C^k[0, 2\pi]$, then the integrands D_j, F_j and H_{ij} in Eq. (3.4) are of $C^{k-1}[0, 2\pi]$, $C^{k-1}[0, 2\pi]$ and $C^{k-2}[0, 2\pi]$, respectively.

It is sufficient to show that $DD(\alpha)$, $F_{ij}(\alpha)$, and $HH(\alpha)$, as defined in (A.3), (A.4), and (A.5), are of $C^{k-1}[0, 2\pi]$, $C^{k-1}[0, 2\pi]$ and $C^{k-2}[0, 2\pi]$, respectively. In the following, we show that $HH(\alpha)$ is of C^{k-2} , while the proof for $DD(\alpha)$ and $F_{ij}(\alpha)$ follows similarly.

It is obvious from (A.5) that $HH(\alpha)$ is of C^{k-1} for any $\alpha \neq \alpha_0$. Then, it remains to show that $HH(\alpha)$ is $(k-2)$ -times differentiable at $\alpha = \alpha_0$. First, let's express $x_i(\alpha) - x_i(\alpha_0)$ in Taylor expansion

$$x_i(\alpha) - x_i(\alpha_0) = x_i'(\alpha)(\alpha - \alpha_0) + g_i(\alpha)(\alpha - \alpha_0)^2, \quad i=1,2, \quad (\text{A.10})$$

where $g_i(\alpha) = x_i''(\xi)/2$ and ξ is some point between α and α_0 . Clearly $g_i(\alpha)$'s are of $C^{k-2}[0,2\pi]$ provided $x_i(\alpha)$'s are of $C^k[0,2\pi]$. Using the expression (A.10), we can write $HH(\alpha)$ defined in (A.5) as

$$HH(\alpha) = \frac{g_1(\alpha)x_2'(\alpha) - g_2(\alpha)x_1'(\alpha)}{[(x_1'(\alpha) + g_1(\alpha)(\alpha - \alpha_0))^2 + (x_2'(\alpha) + g_2(\alpha)(\alpha - \alpha_0))^2]}. \quad (\text{A.11})$$

Now, $HH(\alpha)$ is expressed as a quotient of two $C^{k-2}[0,2\pi]$ functions of α and the denominator equals to $[(x_1'(\alpha_0))^2 + (x_2'(\alpha_0))^2]$ at $\alpha = \alpha_0$, nonzero for a C^2 curve. Thus, we have shown $HH(\alpha)$ is also $(k-2)$ times differentiable at $\alpha = \alpha_0$. This completes the proof.

References

- [1] L. K. Antanovskii, Formation of a pointed drop in Taylor's four-roller mill, *J. Fluid Mech.*, 327 (1996), 325–341.
- [2] J. W. Cahn and J. E. Hilliard, Free energy of a non-uniform system I: interfacial free energy, *J. Chem. Phys.*, 28 (1958), 258–267.
- [3] P. Dimitrakoloupos and J. Wang, A spectral boundary element algorithm for interfacial dynamics in two-dimensional Stokes flow based on Hermitian interfacial smoothing, *Engng. Analy. Bound. Elem.*, 31 (2007), 646–656.
- [4] T. Hou, J. S. Lowengrub and M. J. Shelley, Removing the stiffness from interfacial flows with surface tension, *J. Comput. Phys.*, 114 (1994), 312–338.
- [5] D. Juric and G. Tryggvason, Computations of boiling flows, *Int. J. Multiphas. Flow.*, 24 (3) (1998), 387–410.
- [6] R. Kress, *Linear Integral Equations*, Springer, Second Edition, 1999.
- [7] M. Kropinski, An efficient numerical method for studying interfacial motion in two-dimensional creeping flows, *J. Comput. Phys.*, 171 (2001), 479–508.
- [8] Z. Li and K. Ito, *The Immersed Interface Method: Numerical Solutions of PDEs Involving Interfaces and Irregular Domains*, Society for Industrial and Applied Mathematics, 2006.
- [9] Q. Nie, S. Tanveer, T. Dupont and X. Li, Singularity formation in free-surface Stokes flows, *Contemp. Math.*, 306 (2002), 147–165.
- [10] S. Osher and R. P. Fedkiw, Level set methods: an overview and some recent results, *J. Comput. Phys.*, 169 (2001), 463–502.
- [11] C. S. Peskin, The immersed boundary method, *Acta Numerica.*, 11 (2002), 479–517.
- [12] C. Pozrikidis, *Boundary Integral and Singularity Methods for Linearized Viscous Flow*, Cambridge University Press, 1992.
- [13] C. Pozrikidis, Numerical studies of cusp formation at fluid interfaces in Stokes flow, *J. Fluid. Mech.*, 357 (1998), 29–57.
- [14] C. Pozrikidis, Interfacial dynamics for Stokes flows, *J. Comput. Phys.*, 169 (2) (2001), 250–301.

- [15] Y. Saad and M. H. Schultz, GMRES: a generalized minimal residual algorithm for nonsymmetric linear systems, *SIAM J. Sci. Stat. Comput.*, 7 (1986), 856–869.
- [16] R. Scardovelli and S. Zaleski, Direct numerical simulation of free-surface and interfacial flow, *Ann. Rev. Fluid. Mech.*, 31 (7) (1999), 567–603.
- [17] M. Siegel, Cusp formation for time-evolving bubbles in two-dimensional Stokes flow, *J. Fluid. Mech.*, 412 (2000), 227–257.
- [18] S. Tanveer and G. L. Vasconcelos, Time-evolving bubbles in two-dimensional Stokes flow, *J. Fluid. Mech.*, 301 (1995), 325–344.